HHS Public Access

Author manuscript

Phys Med Biol. Author manuscript; available in PMC 2018 January 07.

Published in final edited form as:

Phys Med Biol. 2017 January 07; 62(1): 202–213. doi:10.1088/1361-6560/62/1/202.

Low Dose Lung Cancer Screening With Photon-Counting CT: A Feasibility Study

Rolf Symons[1], **Tyler Cork**[1], **Pooyan Sahbaee**[2], **Matthew K. Fuld**[2], **Steffen Kappler**[3], **Les R. Folio**[1], **David A. Bluemke**[1], and **Amir Pourmorteza**[1]

[1]Radiology and Imaging Sciences - National Institutes of Health Clinical Center, Bethesda, MD, USA

[2]Siemens Medical Solutions, Malvern, PA, USA

[3]Siemens Healthcare GmbH, Forchheim, Germany

Abstract

Objective—To evaluate the feasibility of using a whole-body photon-counting detector (PCD) CT scanner for low dose lung cancer screening compared to a conventional energy integrating detector (EID) system.

Materials and Methods—Radiation dose-matched EID and PCD scans of the COPDGene 2 phantom were acquired at different radiation dose levels ($CTDI_{vol}$: 3.0, 1.5, and 0.75 mGy) and different tube voltages (120, 100, and 80 kVp). EID and PCD images were compared for quantitative Hounsfield unit accuracy, noise levels, and contrast-to-noise ratios (CNR) for detection of ground-glass nodules (GGN) and emphysema.

Results—The PCD Hounsfield unit accuracy was better than EID for water at all scan parameters. PCD HU stability for lung, GGN and emphysema regions were superior to EID and PCD attenuation values were more reproducible than EID for all scan parameters (all $P<0.01$), while Hounsfield units for lung, GGN and emphysema ROIs changed significantly for EID with decreasing dose (all $P<0.001$). PCD showed lower noise levels at the lowest dose setting at 120, 100 and 80 kVp (15.2±0.3 HU vs 15.8±0.2 HU, P=0.03; 16.1±0.3 HU vs 18.0±0.4 HU, P=0.003; and 16.1±0.3 HU vs 17.9±0.3 HU, P=0.001, respectively), resulting in superior CNR for evaluation of GGNs and emphysema at 100 and 80 kVp.

Conclusion—PCD provided better Hounsfield unit stability for lung, ground-glass, and emphysemaequivalent foams at lower radiation dose settings with better reproducibility than EID. Additionally, PCD showed up to 10% less noise, and 11% higher CNR at 0.75 mGy for both 100 and 80 kVp. PCD technology may help reduce radiation exposure in lung cancer screening while maintaining diagnostic quality.

Keywords

computed tomography; photon-counting CT; lung imaging; low dose CT; image quality; lung cancer screening; ground-glass nodule; emphysema; low-contrast detectability

Authors who are not employees of or consultants for Siemens had control of inclusion of any data and information that might present a conflict of interest for the authors who are employed by Siemens.

1. Introduction

Lung cancer is the leading cause of cancer-related mortality worldwide (Jemal *et al 2011*). At the time of initial diagnosis, lung cancer is often already advanced, resulting in poor 5-year survival rates of only 17.4%. Therefore, earlier detection of lung cancer with low-dose computed tomography (CT) lung cancer screening became a focus of research in radiology. The National Lung Screening Trial (NLST) was the largest randomized controlled trial to demonstrate a significant reduction in lung cancer specific and all-cause mortality with CT screening (Team NLST 2011). However, the diagnostic benefits of lung cancer screening have to be balanced with the inherent risks of ionizing radiation, and overdiagnosis and work-up of false positive findings (Mayo *et al* 2003). Accordingly, major efforts are being made to reduce radiation dose of CT screening, while maintaining diagnostic imaging quality.

Photon-counting detectors (PCDs) use semiconductors to directly convert X-rays into electronic signals. Impinging X-rays create electron-hole pairs, and a strong electric field causes separation of those charges. The fast drifting electron clouds induce short charge pulses of a few nanoseconds on signal pads, which again are registered by front-end electronics. A pulse shaping circuit transforms the charge pulses into voltage pulses. Their pulse-height is approximately proportional to the total charge of the corresponding electron clouds, and therefore indicates the energies of the incident X-rays. Physics effects like Compton scattering, K-escape, charge trapping or charge sharing among neighbor pixels deteriorate the incoming X-ray energy spectra and transform them into pulse-height spectra (Guerra *et al* 2008, Xu *et al* 2011, Taguchi and Iwanczyk 2013, Cammin *et al* 2014). High-speed application specific integrated circuits (ASICs) sample the pulse-height spectra. Multiple counters register the number of signal pulses exceeding different pulse-height thresholds.

Conventional energy-integrating detectors (EIDs) measure the x-ray intensity, which is the combined effect of the count and energy of x-ray photons, by summing the total energy deposited by multiple photons in a time interval. PCDs on the other hand, measure the energy and number of photons separately; while the detector readout noise affects the pulse-height (energy of incident photons) it does not affect the number of pulses (photon count) and therefore, electronic detector readout noise and swank noise are effectively eliminated in photon counts but they are present in the spectral information (Taguchi and Iwanczyk 2013, Tanguay *et al* 2010). The absence of classical detector readout noise preserves the quantum statistics of the measured x-ray photons. This enables a further reduction in image noise especially in scans with low photon statistics (Weidinger *et al* 2012).

It is well established that PCDs enhance contrast in CT images by providing spectral information in the form of two or more energy bins that may be used in k-edge imaging, energy image-based weighting(Schmidt 2009, Weidinger *et al* 2013), and material decomposition (Alvarez and Macovski 1976, Lehmann and Alvarez 1986, Schlomka *et al* 2008, Iwanczyk *et al* 2009, Kappler *et al* 2013, Lee *et al* 2014).

However, non-spectral advantages of PCDs are less investigated (Weidinger *et al* 2012). Individual detection of photons provides better weighting for low-energy photons, which carry more contrast between soft tissue, and are not detected individually in EIDs (Taguchi and Iwanczyk 2013). As a result, even without using the energy information, PCDs may provide better soft tissue contrast, and reduce beam hardening artifacts (Pourmorteza *et al* 2016).

This is especially advantageous in low-dose scan protocols in which the total number of photons is limited and spectral grouping of detected photons will result in photon-starved energy bins. Therefore, even without spectral information, PCDs have the potential to improve the riskbenefit ratio of lung-cancer screening by further reducing the radiation dose and increasing softtissue contrast.

The purpose of this study was to evaluate the performance of a whole-body PCD CT scanner in non-spectral mode for lung cancer screening in a specialized lung tissue phantom with respect to a conventional EID CT system.

2. Methods

2.1. Test object description

The COPDGene 2 test object (Phantom Laboratories, Salem, NY, USA) was developed by the COPDGene Imaging Committee in collaboration with the National Institute of Standards (NIST) (Gaithersburg, MD, USA). The test object consists of an outer ring with x-ray attenuation characteristics similar to water and an inner ring with x-ray attenuation similar to the attenuation of normal lung tissue (-856 HU) (Figure 1) (Sieren *et al* 2012). The inner ring contains additional inserts that can be used for a quantitative densitometry study: 20-lb NIST foam (-703 HU), water (0 HU), 12-lb NIST foam (-824 HU), acrylic (120 HU), 4-lb NIST foam (-937 HU), lung-equivalent foam (-856 HU), and air (-1000 HU). The reference values are based on a typical EID scan acquired at 120 kVp. Significant differences in the CT attenuation measurements of the test object as a function of different characteristics of individual CT scanners have been shown. However, for an individual scanner, the reproducibility of the test object can be reliably assessed and be used to compare the accuracy of the EID and PCD in our prototype scanner (Sieren *et al* 2012). The COPDGene 2 test object has been validated as a reference standard for CT attenuation assessment and encompasses the range of densities important in CT lung cancer screening. Additionally, the test object contains 12 internal air holes and six polycarbonate tubes to simulate different airway sizes.

2.2. CT imaging system

We evaluated a hybrid research prototype CT scanner that is not commercially available. The scanner is equipped with two measurement systems. One is a CdTe-based PCD and the other one is a conventional GOS-based EID. It uses a CT gantry from a commercially available clinical CT scanner (SOMATOM Definition Flash, Siemens Healthcare GmbH, Forchheim, Germany). It has two independent fan-beam systems at an angle of 95 degrees with mountings for CT detectors. The prototype scanner has a 78 cm wide bore, each X-ray

system has a source-to-axis and source-to-detector distances of 595 mm and 1085.6 mm, respectively. The scanner can be operated at rotation times of 0.5 s and 1.0 s per revolution. The X-ray tubes can be operated at 80 kV, 100 kV, 120kV, and 140kV. The tube current can be set to values between 25 mA and 550 mA (in steps of 1 mA).

The counting detector consists of 30 modules, each designed to support two tiles of 64×64 square sub-pixels at 225 μm pitch. This yields an effective field-of-view (FOV) of 27.5 cm which was sufficient for lung imaging. The thickness of the CdTe-based sensor material is chosen to 1.6 mm in order to provide an X-ray stopping power similar to common CT scanners. Currently, the detector can be read out channel-by-channel (for calibration purposes) and in channel groups of 4x4 sub-pixels (for imaging purposes). The latter configuration corresponds to the geometry of the anti-scatter collimator mounted on top of the direct converter. This so-called macro-pixel mode yields CT-typical effective pixel sizes of 0.9×0.9 mm^2 active area and 1.1×0.9 mm^2 pitch at the detector. The resulting intrinsic slice thickness amounts to 0.5 mm at the iso-center. The PCD system can be operated with collimations of 20 or 32 macro-pixel rows, providing a maximum zcoverage of 16 mm at the iso-center.

Every sub-pixel features two counters with individually adjustable thresholds. Each counter registers the number of pulses that are above their set threshold. In this study, we adjusted the PCD energy thresholds to 25 keV and 75 keV. We used the image reconstructed from all detected photons with energies above 25 keV threshold when comparing PCD to EID. The 75 keV threshold was chosen arbitrarily and was not used in this study; as mentioned in Introduction, the scope of this study was to investigate the non-spectral properties of PCDs, without grouping the detected photons into energy bins.

The EID is unchanged with respect to the commercial scanner. It consists of a 1.4 mm thick scintillating X-ray converter of GOS which is coupled to photodiodes and read out by chargeintegrating electronics. With a pitch of 1.2×1.0 mm^2 these pixels are slightly larger than the macro-pixels of the counting detector. The detector covers a full FOV of 50 cm, has 64 pixel rows and provides an intrinsic slice thickness of 0.6 mm at the iso-center. Further details of regarding the design of the prototype scanner (including the macro- and sub-pixel geometry) and its imaging performance can be found in (Kappler *et al* 2014, Yu *et al* 2016).

2.3. CT scan protocol

The test object was fixed in the isocenter of the field-of-view with its long axis parallel to the CT gantry along the x-y plane of the detectors, consistent with routine clinical scanning protocols. EID and PCD spiral scans of the test object were acquired at 3 different predefined volume CT dose index ($CTDI_{vol}$) settings (3.0, 1.5, and 0.75 mGy for 100 and 80 kVp, and 3.0, 1.5, and 0.97 mGy for 120 kVp). The lowest dose setting at 120 kVp was slightly higher as no lower tube current can be prescribed on the prototype at this moment. Corresponding dose-length products (DLPs) for an average length human thorax (30 cm) at 80 or 100 kVp would be 90, 45, and 22.5 mGy.cm for the three CTD_{Ivol} settings, respectively. With the same tube current (mAs), $CTDI_{vol}$ estimates for the PCD were 10% higher than the estimates for the EID detector. However, this is not a limitation of the PCD technology and can be attributed to the different shape of x-ray beam profile and detector

collimation along z-axis (Dixon 2003). Therefore, the tube current value corresponding with the predefined $CTDI_{vol}$ settings for the EID system was matched for the PCD system. This way the number of photons reaching the detector is as similar as possible for both systems allowing for a fair comparison. Spiral pitch was set at 0.8 with a gantry rotation time of 0.5 seconds for both systems. Each acquisition was repeated 5 times to assess reproducibility of the measurements.

2.4. Image reconstruction and analysis

All images were reconstructed by using sinogram-affirmed iterative reconstruction (SAFIRE) algorithm with ReconCT (v13.8.4.0, Siemens Healthcare, Erlangen, Germany). For each phantom acquisition, the EID and PCD projections were reconstructed at 1 mm slice thickness with 1 mm increment and a medium smooth quantitative kernel (Q30) with SAFIRE strength 3. All reconstructions were performed with FOV of 275 mm and matrix size of 512×512 pixels. Quantitative HU stability and reproducibility of the EID and PCD system were evaluated in 7 paired circular ~3.8 cm^2 regions of interest (ROIs) centered in each material in the test object. As mentioned in the introduction section, EIDs and PCDs have different intrinsic energy weighting of detected photons, which may lead to different attenuation values. Therefore, we do not expect the HU values of the EID and PCD images to be the similar to each other (or to the phantom manufacturer's reported values) except in the water and air ROIs, where the HU accuracy was measured as HU difference from 0 and -1000 for water and air, respectively. Hounsfield unit stability was defined as the absolute difference between the mean HU value of each ROI measured at the highest CTDIvol and the lower dose scans of each detector system for each kVp setting.

The standard deviation (SD) of the HU values of each ROI was used as a measure of image noise. Detection of ground-glass nodules (GGN) and emphysema is a challenging task for lowdose lung cancer screening because GGNs have a low lesion-to-background contrast. The typical densities of GGNs and emphysema vary between -650 and -800 HU, and -850 and -1000 HU, respectively (Funama *et al* 2009). Therefore, we used the 20-lb (-703 HU) and 4-lb (-937 HU) NIST foam regions of the phantom for CNR analysis of GGNs and emphysema, respectively. Contrast-to-noise ratio (CNR) for detection of GGN and emphysema was calculated as $CNR_X = |\mu_X - \mu_{Lung}|/\sigma_{Lung}$, where μ, σ are the mean and standard deviation of Hounsfield units in the corresponding ROIs and X can refer to GNN or emphysema. All CNR measurements were performed on the center slice of the test object to simulate routine clinical reading with thin axial slices. All HU values mentioned in this section are nominal for a 120 kVp scan.

2.5. Statistical analysis

Statistical analyses were performed using R Statistical Software (Foundation for Statistical Computing, v.3.2.2, Vienna, Austria). Continuous data were expressed as means with standard deviations. Welch paired t-test was used to compare continuous variables between EID and PCD. F test of variance was used to compare reproducibility of repeat scans. Repeated-measures analysis of variance or Wilcoxon signed-rank test (paired) with post hoc Bonferroni corrected pairwise comparison was used as appropriate to compare attenuation

accuracy, noise and CNR values between different dose settings. Statistical significance was defined at a P-value of <0.05. All measurements are reported as mean ± SD.

3. Results

3.1. Hounsfield unit stability

Attenuation values of the test object materials at all kVp and dose levels are summarized in Table 1. PCD attenuation values were significantly more consistent and reproducible between the 5 repeat scans for all tube voltage and dose settings, as reflected by the smaller SD of all measurements in PCD (all P<0.01).Additionally, PCD attenuation stability was better for lung, GGN, and emphysema equivalent foams: with decreasing dose, attenuation values of EID changed significantly, while attenuation values of PCD remained unchanged (Figure 2). PCD showed more accurate Hounsfield unit values than EID for water at all radiation dose levels and tube voltages. In contrast, EID attenuation accuracy was better for air at all dose levels and tube voltages. PCD attenuation values for water increased for the lowest dose setting (0.75 mGy) at 80 and 100 kVp. Nevertheless, PCD water values remained more accurate than those obtained by EID. Attenuation values for acrylic and air were not significantly influenced by dose changes. Tube voltage changes significantly changed EID and PCD attenuation values of acrylic and PCD attenuation values of water at 100 and 80 kVp (all P<0.001).

3.2. Image noise and CNR

As we expected, image noise increased with decreasing dose levels at all tube voltages for both EID and PCD (all P<0.001). Figure 3 summarizes noise values for the lung foam for different tube voltages and dose settings. PCD showed lower noise levels compared with EID for the lowest dose setting (0.75 mGy) at 120, 100 and 80 kVp (15.2±0.3 HU vs 15.8±0.2 HU, P=0.03; 16.1±0.3 HU vs 18.0 ± 0.4 HU, P=0.003; and 16.1±0.3 HU vs 17.9±0.3 HU, P=0.001, respectively, see Online appendix). Tube voltage setting did not affect noise levels for both EID and PCD. At the lowest dose setting, noise levels for 120 kVp were significantly lower than those for 100 and 80 kVp, though this should be attributed to the slightly higher dose for 120 kVp (0.97 mGy) at this lowest dose level as lower dose scanning at 120 kVp is not possible on the prototype. Similar noise levels were obtained for the other test object materials.

Contrast-to-noise ratios (CNR) for the detection of GGN and emphysema were significantly higher for PCD than EID at the lowest dose setting (0.75 mGy) at both 100 (GGN: 9.8 ± 0.2 vs 9.4 ± 0.2, P=0,02; emphysema: 4.9 ± 0.1 vs 4.5 ± 0.1, P=0.01, respectively) and 80 kVp (GGN: 9.9 ± 0.1 vs 9.5 ± 0.2, P=0.01; emphysema: 4.9 ± 0.1 vs 4.4 ± 0.2, P=0.002, respectively, see Online appendix). Different tube voltage settings did not significantly affect CNR (the 120 kVp higher CNR at the lowest dose setting is due to the slightly higher dose as previously mentioned). CNR results are shown in Figure 4.

4. Discussion

This study reports the feasibility of low-dose lung cancer screening CT scans using a whole-body photon counting detector CT scanner and is the first to demonstrate superior

performance of PCD technology compared to state-of-the-art EID technology. In the COPDgene phantom, PCD detectors showed superior HU stability and reproduciblity to EID detectors for water, lung, GGN, and emphysema, especially at lower dose settings. Improved HU stability and reproducibility of PCD images may be attributed to the absence of electronic noise in photon counts. Additive electronic noise in EID causes bias in HU values.

As mentioned in Introduction, effective elimination of electronic noise and better low-energy photon weighting in PCDs result in lower image noise and higher soft tissue contrast, which in turn lead to improved soft tissue CNR and higher dose efficiency of PCD technology. The noise reduction and HU stability were specifically significant at the lowest CTDI setting where electronic noise becomes more prominent in EID. Noise levels for lung foam were up to 11% lower for PCD at 0.75 mGy for all tube voltages. The contrast improvement was more prominent in lower kVps, whose spectrums contain a larger portion of low-energy photons. In particular, PCD had superior CNRs for the detection of GGNs and emphysema at 100 and 80 kVp on the lowest dose setting. This makes photon-counting CT a promising technique in radiation dose reduction, critical in further improving the benefit-risk ratio of CT lung cancer screening. This paper focused on the non-spectral aspect of PCDs, due to the low number of photons used in imaging. A potential advantage of PCD, which was not investigated here, is the spectral information obtained without misregistration to enhance soft-tissue differentiation with or without iodine contrast agents.

Recent efforts from a variety of industry standards groups including the Quantitative Imaging Biomarkers Alliance (QIBA) have endeavored to tackle the issue of HU variability between imaging vendors and scanning platforms (Mulshine *et al* 2015). The detection of GGNs and emphysema are important and challenging tasks, however, the next step after detection is to provide quantitative metrics that can be used to evaluate and assess disease progression; this task is complicated by the HU variability between systems. In certain diseases, even a 1 HU change may be clinically significant to demonstrate disease progression, as with alpha1-antitrypsin deficiency (Stoel *et al* 2008). Thus efforts at improved accuracy for lung density ascertainment is necessary to provide quantitative biomarkers for the further development of treatments for diseases such as emphysema and idiopathic pulmonary fibrosis (IPF) that are currently characterized by HU changes. The use of PCD technology shows great promise in HU stability even at the lowest doses and may provide an additional advantage for quantitative imaging in the future.

There are several limitations of the current study. The current CT prototype lacks a tin filter and model-based iterative reconstruction. By using that technology, prior studies have shown that the radiation dose could be lowered even further (Newell Jr *et al* 2015). Filtered-backprojection (FBP) reconstructions of the current data, resulted in images that were not of diagnostic quality due to excessive noise and image artifacts. It has been shown that truncation of Hounsfield scale at -1024 HU causes paradoxical reduction of standard deviation and shifts mean HU towards more positive values, especially for regions with HU values close to air e.g. lung tissue (Sieren *et al* 2014). Use of SAFIRE algorithm reduces the noise and lowers the effect of HU truncation; however, it may limit generalization of these results to other scanners. An additional limitation is that the current study is limited to phantoms without in vivo correlation.

In this study, the EID system had larger effective detector size compared to PCD (0.6×0.6 mm vs 0.5×0.5 mm at isocenter) do to the limitations of the prototype scanner, therefore the intrinsic slice thickness and image voxel size were larger for EID than PCD; at similar photon flux, reducing the EID pixel size to 0.5 mm would reduce the incident x-ray intensity and therefore increase the effect of electronic detector noise on the projections. Despite, this advantage of the EID system, PCD still outperformed in terms of image noise.

We used data acquired from 4×4 binned detector macropixels. While pixel binning may reduce the effects of charge sharing, it has been shown that reconstruction of unbinned data can reduce image noise (Baek *et al* 2013). However, due to the limited bandwidth of the data transfer hardware it was not possible to acquire unbinned data in imaging mode. This limitation of the prototype is going to be removed in the next stage of development. The task-specific trade-off between charge sharing effect and image noise reduction through binning of PCD sub-pixels merits further investigation.

Pulse pile-up may affect count linearity in PCD images. This effect occurs when the incident xray photons are too close in time to be counted by the PCD counters separately, and are counted as one photon. This will cause an increase in HU and quantum noise. The current implementation of PCD technology with its high-speed application specific integrated circuits (ASICs) and very small sub-pixel size have been shown to be robust to pulse pileup artifacts at elevated tube currents (Kappler *et al* 2014). Yu et al have investigated the impact of high photon flux on image quality of a similar system in detail and reported that the effect is not “perceptible” in this PCD up to photon flux 300 mAs and was still negligible at 550 mAs, in a small neonate water phantom (Yu *et al* 2016). In this study we used tube current-time settings below 30 mAs, and therefore no pulse pile-up artifact was expected nor observed.

In summary, this study reports the feasibility of photon counting low dose lung cancer screening CT. Photon counting CT provided better Hounsfield unit accuracy for water, lung, ground-glass, and emphysema foams. The photon counting detector system showed less noise and higher CNR compared with the conventional EID. Therefore, photon counting technology may help further reduce dose in lung cancer screening while maintaining diagnostic quality.

Acknowledgments

This study was supported by the NIH intramural research program (ZIACL090019; ZIAEB000072), and in part by a collaborative research agreement with Siemens Medical Systems (Forchheim, Germany).

References

Alvarez RE, Macovski A. Energy-selective reconstructions in x-ray computerised tomography. Phys Med Biol. 1976; 21:733. [PubMed: 967922]

Baek J, Pineda AR, Pelc NJ. To bin or not to bin? The effect of CT system limiting resolution on noise and detectability. Phys Med Biol. 2013; 58:1433. [PubMed: 23399724]

Cammin J, Xu J, Barber WC, Iwanczyk JS, Hartsough NE, Taguchi K. A cascaded model of spectral distortions due to spectral response effects and pulse pileup effects in a photon-counting xray detector for CT. Med Phys. 2014; 41:41905.

Dixon RL. A new look at CT dose measurement: beyond CTDI. Med Phys. 2003; 30:1272–80. [PubMed: 12852553]

Funama Y, Awai K, Liu D, Oda S, Yanaga Y, Nakaura T, Kawanaka K, Shimamura M, Yamashita Y. Detection of nodules showing ground-glass opacity in the lungs at low-dose multidetector computed tomography: phantom and clinical study. J Comput Assist Tomogr. 2009; 33:49–53. [PubMed: 19188784]

Guerra P, Santos A, Darambara DG. Development of a simplified simulation model for performance characterization of a pixellated CdZnTe multimodality imaging system. Phys Med Biol. 2008; 53:1099. [PubMed: 18263961]

Iwanczyk JS, Nygård E, Meirav O, Arenson J, Barber WC, Hartsough NE, Malakhov N, Wessel JC. Photon counting energy dispersive detector arrays for x-ray imaging. Nucl Sci IEEE Trans. 2009; 56:535–42.

Jemal A, Bray F, Center MM, Ferlay J, Ward E, Forman D. Global cancer statistics. CA Cancer J Clin. 61:69–90.

Kappler S, Henning A, Krauss B, Schoeck F, Stierstorfer K, Weidinger T, Flohr T. Multi-energy performance of a research prototype CT scanner with small-pixel counting detector. SPIE Medical Imaging (International Society for Optics and Photonics). 2013:86680O–86680O.

Kappler S, Henning A, Kreisler B, Schoeck F, Stierstorfer K, Flohr T. Photon counting CT at elevated X-ray tube currents: contrast stability, image noise and multi-energy performance. 2014; 9033:90331C–90331C - 8.

Lee S, Choi Y-N, Kim H-J. Quantitative material decomposition using spectral computed tomography with an energy-resolved photon-counting detector. Phys Med Biol. 2014; 59:5457. [PubMed: 25164993]

Lehmann LA, Alvarez RE. Energy-selective radiography a review. Digital Radiography (Springer). 1986:145–88.

Mayo JR, Aldrich J, Muller NL. Radiation exposure at chest CT: a statement of the Fleischner Society 1. Radiology. 2003; 228:15–21. [PubMed: 12832569]

Mulshine JL, Gierada DS, Armato SG, Avila RS, Yankelevitz DF, Kazerooni EA, McNitt-Gray MF, Buckler AJ, Sullivan DC. Role of the quantitative imaging biomarker alliance in optimizing ct for the evaluation of lung cancer screen–detected nodules. J Am Coll Radiol. 2015; 12:390–5. [PubMed: 25842017]

Newell JD Jr, Fuld MK, Allmendinger T, Sieren JP, Chan K-S, Guo J, Hoffman EA. Very low-dose (0.15 mGy) chest CT protocols using the COPDGene 2 test object and a third-generation dual-source CT scanner with corresponding third-generation iterative reconstruction software. Invest Radiol. 2015; 50:40. [PubMed: 25198834]

Pourmorteza A, Symons R, Sandfort V, Mallek M, Fuld MK, Henderson G, Jones EC, Malayeri AA, Folio LR, Bluemke DA. Abdominal Imaging with Contrast-enhanced Photon-counting CT: First Human Experience. Radiology. 2016; 279:239–45. [PubMed: 26840654]

Schlomka, Jp; Roessl, E.; Dorscheid, R.; Dill, S.; Martens, G.; Istel, T.; Bäumer, C.; Herrmann, C.; Steadman, R.; Zeitler, G. Experimental feasibility of multi-energy photon-counting K-edge imaging in preclinical computed tomography. Phys Med Biol. 2008; 53:4031. [PubMed: 18612175]

Schmidt TG. Optimal “image-based” weighting for energy-resolved CT. Med Phys. 2009; 36:3018–27. [PubMed: 19673201]

Sieren JP, Hoffman EA, Fuld MK, Chan KS, Guo J, Newell JD Jr. Sinogram Affirmed Iterative Reconstruction (SAFIRE) versus weighted filtered back projection (WFBP) effects on quantitative measure in the COPDGene 2 test object. Med Phys. 2014; 41:91910.

Sieren JP, Newell JD Jr, Judy PF, Lynch DA, Chan KS, Guo J, Hoffman EA. Reference standard and statistical model for intersite and temporal comparisons of CT attenuation in a multicenter quantitative lung study. Med Phys. 2012; 39:5757–67. [PubMed: 22957640]

Stoel BC, Bode F, Rames A, Soliman S, Reiber JHC, Stolk J. Quality control in longitudinal studies with computed tomographic densitometry of the lungs. Proc Am Thorac Soc. 2008; 5:929–33. [PubMed: 19056719]

Taguchi K, Iwanczyk JS. Vision 20/20: Single photon counting x-ray detectors in medical imaging. Med Phys. 2013; 40:100901. [PubMed: 24089889]

Tanguay J, Kim HK, Cunningham IA. The role of x-ray Swank factor in energy-resolving photon-counting imaging. Med Phys. 2010; 37:6205–11. [PubMed: 21302777]

Team NLSTR. Reduced lung-cancer mortality with low-dose computed tomographic screening. N Engl J Med. 2011; 365:395. [PubMed: 21714641]

Weidinger T, Buzug TM, Flohr T, Fung GSK, Kappler SG, Stierstorfer K, Tsui BMW. Investigation of ultra low-dose scans in the context of quantum-counting clinical CT. SPIE Medical Imaging (International Society for Optics and Photonics). 2012:83134B–83134B.

Weidinger T, Buzug TM, Flohr T, Kappler S, Schöck F, Stierstorfer K. Threshold optimization for efficient contrast imaging with quantum counting CT detectors. SPIE Medical Imaging (International Society for Optics and Photonics). 2013:86680Q–86680Q.

Xu C, Danielsson M, Bornefalk H. Evaluation of energy loss and charge sharing in cadmium telluride detectors for photon-counting computed tomography. Nucl Sci IEEE Trans. 2011; 58:614–25.

Yu Z, Leng S, Jorgensen SM, Li Z, Gutjahr R, Chen B, Halaweish AF, Kappler S, Yu L, Ritman EL. Evaluation of conventional imaging performance in a research whole-body CT system with a photon-counting detector array. Phys Med Biol. 2016; 61:1572. [PubMed: 26835839]

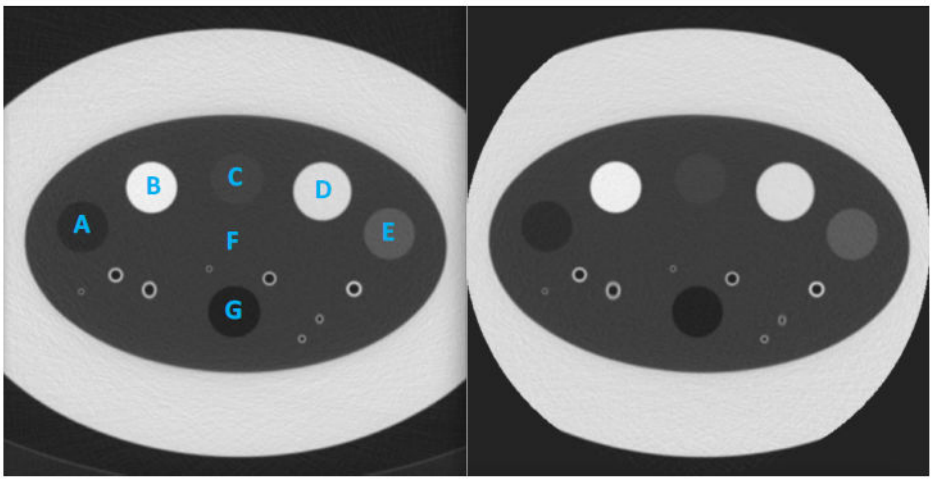

Figure 1.

EID (A) and PCD (B) scans of the COPDGene 2 phantom. The 7 calibrated test object materials regions-of-interest (ROIs) used for analysis are labeled: A, emphysema foam; B, acrylic; C, 12-lb foam; D, water; E, ground-glass nodule foam; F, lung foam; G, air.

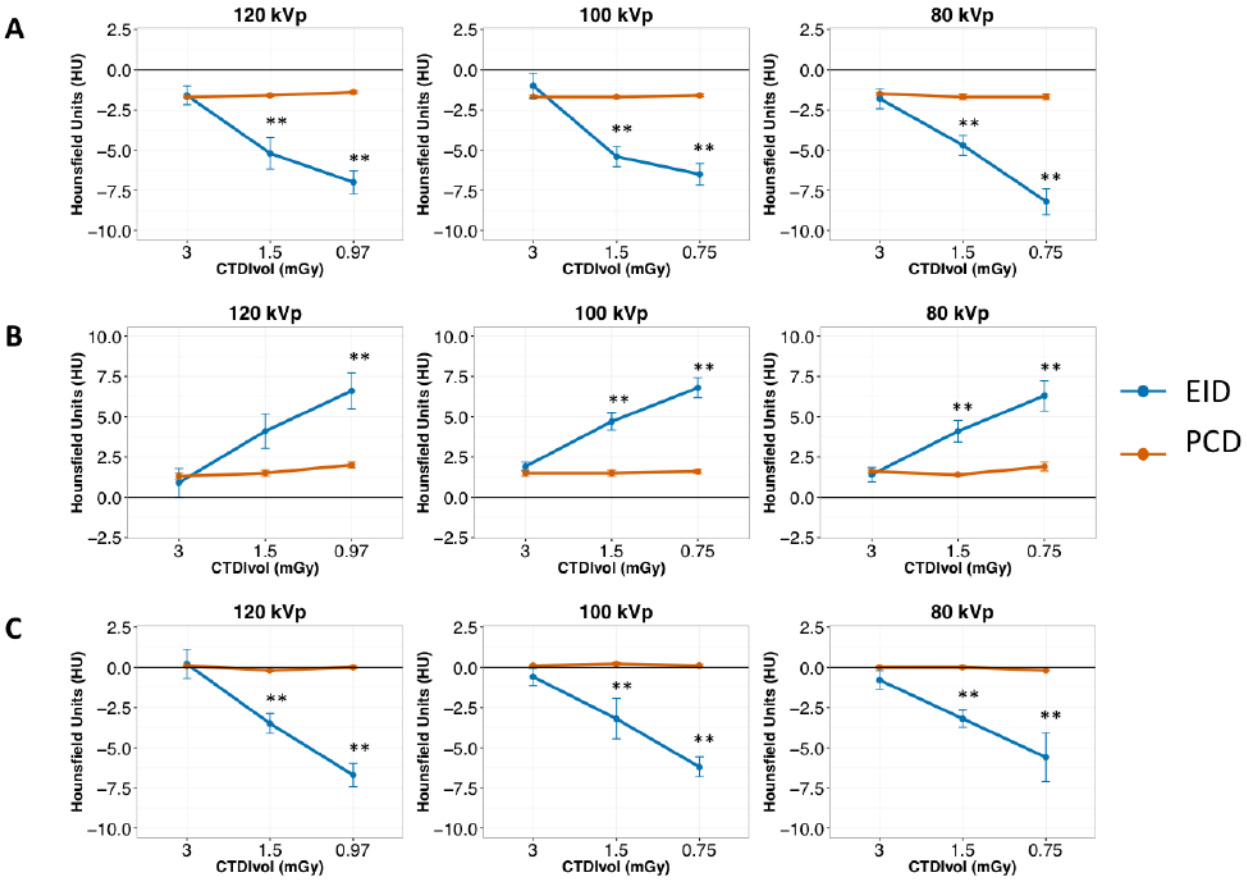

Figure 2.

Hounsfield unit (HU) accuracy with standard error of the mean (SEM) for lung (A), ground-glass nodules (B), and emphysema (C) equivalent foams of the COPDGene 2 phantom for EID and PCD at different dose levels. For better visualization, the measured values are subtracted from nominal HU values reported by the phantom manufacturer at 120 kVp. EID HU accuracy was inferior to PCD at 1.5 and 0.75 mGy CTDIvol dose levels. **: P<0.05.

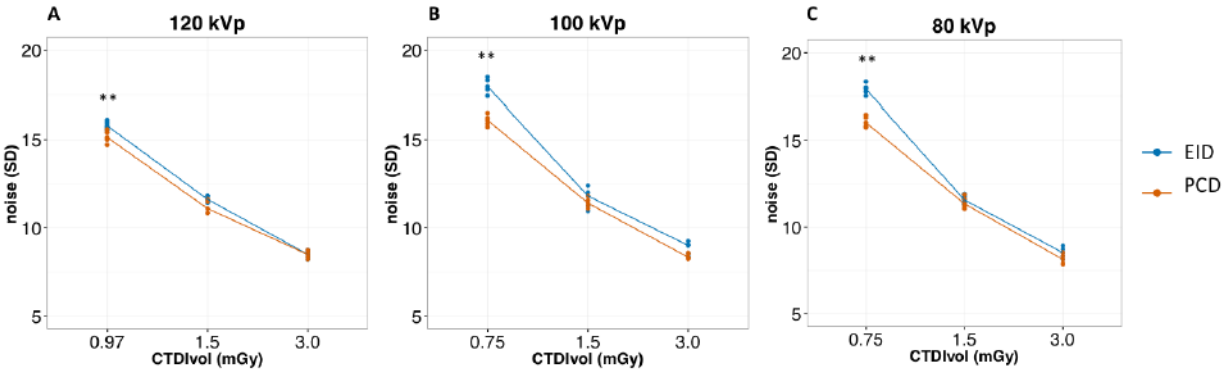

Figure 3.

Image noise of SAFIRE 3 Q30f reconstructions of the COPDGene 2 phantom at different tube voltages. Dots represent the noise levels for individual repetitions at each dose level. Lines connect the average noise levels for EID (blue) and PCD (red) at each dose level. PCD noise was significantly lower than EID at the lowest dose setting for all tube voltages. **: $P<0.05$.

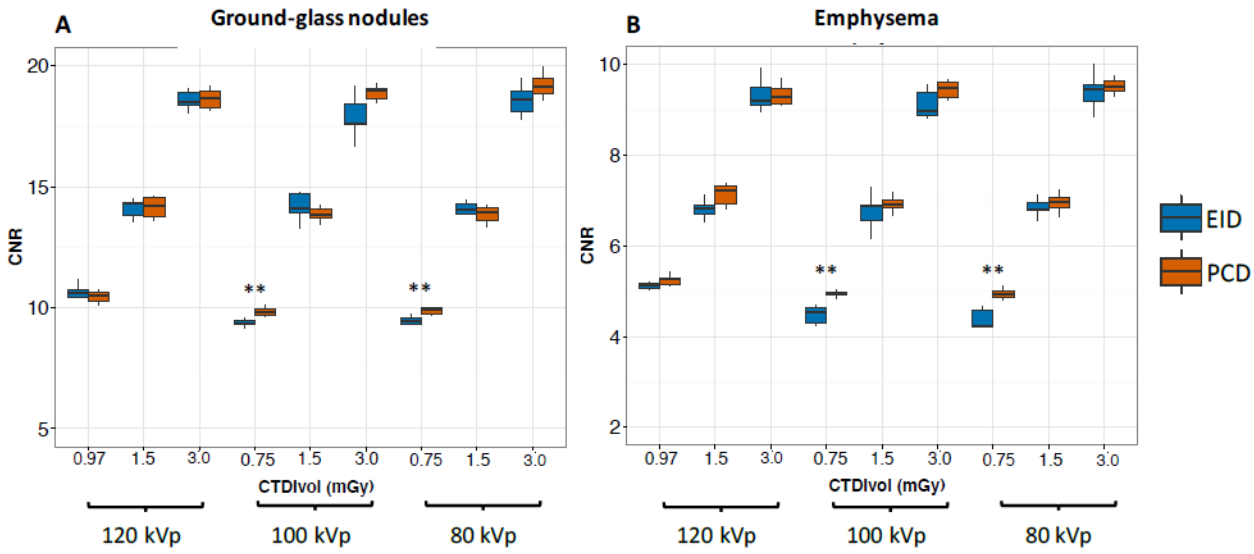

Figure 4.

Contrast-to-noise ratios (CNR) for the detection of ground-glass nodules (A) and emphysema (B). CNR for both ground-glass nodules and emphysema was significantly higher for PCD (red) than EID (blue) for the lowest dose setting at 100 and 80 kVp. **: $P<0.05$

Table 1

Mean attenuation values and SD of the test object materials at different tube voltages and $CTDI_{vol}$ dose levels

Tube voltage	**120 kVp**		**100 kVp**		**80 kVp**	
Acrylic (120 HU)	**EID**	**PCD**	**EID**	**PCD**	**EID**	**PCD**
3.0 mGy	119.1±1.3	118.1±0.1	111.1±1.6	110.2±0.1	99.0±1.4	99.3±0.2
1.5 mGy	119.4±1.6	118.4±0.2	111.0±2.1	110.2±0.1	98.8±1.6	99.0±0.1
0.75 mGy *	118.7±1.5	118.3±0.2	110.4±1.4	110.1±0.2	99.1±1.4	99.3±0.1
P-value	0.79	0.06	0.57	0.81	0.93	0.98
Water (0 HU)	**EID**	**PCD**	**EID**	**PCD**	**EID**	**PCD**
3.0 mGy	-8.0±1.5	-4.1±0.1	-8.5±1.5	-4.2±0.2	-7.9±1.5	-4.3±0.4
1.5 mGy	-8.3±1.5	-3.7±0.3	-8.7±1.6	-4.7±0.4	-8.7±1.8	-4.9±0.3
0.75 mGy *	-8.7±1.6	-4.1±0.3	-10.5±1.9	-6.9±0.2 *1,2*	-9.8±.1.7	-7.3±0.2 *1,2*
P-value	0.51	0.56	0.12	<0.001	0.10	<0.001
Emphysema foam (-937 HU)	**EID**	**PCD**	**EID**	**PCD**	**EID**	**PCD**
3.0 mGy	-936.8±2.0	-936.9±0.1	-937.6±1.2	-936.9±0.1	-937.8±1.3	-937.0±0.1
1.5 mGy	-940.5±1.4	-937.2±0.2	-940.2±2.8	-936.8±0.2	-940.2±1.2	-937.0±0.2
0.75 mGy *	-943.7±1.6 *1,2*	-937.0±0.2	-943.2±1.4 *1*	-936.9±0.2	-942.6±3.4 *1*	-937.2±0.1
P-value	<0.001	0.24	<0.001	0.60	0.005	0.14
Lung foam (-856 HU)	**EID**	**PCD**	**EID**	**PCD**	**EID**	**PCD**
3.0 mGy	-857.6±1.3	-857.7±0.2	-857.0±1.7	-857.7±0.3	-857.8±1.4	-857.5±0.2
1.5 mGy	-861.2±2.2 *1*	-857.6±0.4	-861.4±1.4 *1*	-857.7±0.2	-860.7±1.4 *1*	-857.7±0.4
0.75 mGy *	-863.0±1.6 *1*	-857.4±0.2	-862.5±1.5 *1*	-857.6±0.2	-864.2±1.8 *1,2*	-857.7±0.4
P-value	<0.001	0.11	<0.001	0.39	<0.001	0.27
12-lb NIST foam (-824 HU)	**EID**	**PCD**	**EID**	**PCD**	**EID**	**PCD**
3.0 mGy	-823.5±1.5	-823.3±0.2	-824.7±1.8	-823.5±0.1	-824.6±1.3	-823.3±0.2
1.5 mGy	-820.6±1.6 *1*	-823.7±0.2	-821.0±1.5 *1*	-823.5±0.1	-820.7±1.4 *1*	-823.4±0.4

Tube voltage	120 kVp		100 kVp		80 kVp	
Acrylic (120 HU)	**EID**	**PCD**	**EID**	**PCD**	**EID**	**PCD**
0.75 mGy*	-816.8±2.3[1]	-823.6±0.2	-818.2±1.3[1]	-823.4±0.1	-818.2±1.0[1]	-823.3±0.4
P-value	<0.001	0.05	<0.001	0.39	<0.001	0.73
GGN foam (-703 HU)	**EID**	**PCD**	**EID**	**PCD**	**EID**	**PCD**
3.0 mGy	-702.1±2.0	-701.7±0.5	-701.1±1.6	-701.5±0.4	-701.6±1.0	-701.4±0.2
1.5 mGy	-698.9±2.4	-701.5±0.4	-698.3±1.2	-701.5±0.4	-698.9±1.5[1]	-701.6±0.2
0.75 mGy*	-696.4±2.5[1]	-701.0±0.4	-696.2±1.4[1]	-701.4±0.3	-696.7±2.1[1,2]	-701.1±0.6
P-value	0.002	0.07	<0.001	0.82	<0.001	0.43
Air (-1000 HU)	**EID**	**PCD**	**EID**	**PCD**	**EID**	**PCD**
3.0 mGy	-999.6±2.9	-995.8±0.1	-998.7±1.2	-995.9±0.1	-999.3±1.7	-995.7±0.5
1.5 mGy	-999.3±2.2	-995.8±0.5	-998.7±1.6	-995.8±0.1	-999.0±1.7	-995.7±0.1
0.75 mGy*	-999.0±1.9	-995±0.2	-998.9±1.4	-995.8±0.1	-998.8±1.4	-995.5±0.2
P-value	0.69	0.59	0.83	0.19	0.61	0.47

[1] post hoc Bonferroni corrected testing <0.05 versus 120 kVp;

[2] post hoc Bonferroni corrected testing <0.05 versus 100 kVp.

* 0.97 mGy for 120 kVp.